Acta Crystallographica Section F
**Structural Biology and Crystallization Communications**
ISSN 1744-3091

# Expression, purification, crystallization and preliminary crystallographic analysis of BipD, a component of the *Burkholderia pseudomallei* type III secretion system

**Pietro Roversi,[a] Steven Johnson,[a] Terry Field,[b] Janet E. Deane,[a] Edouard E. Galyov[b] and Susan M. Lea[a,c]***

[a]Laboratory of Molecular Biophysics, Department of Biochemistry, University of Oxford, South Parks Road, Oxford OX1 3QU, England, [b]Division of Microbiology, Institute for Animal Health, Compton Laboratory, Berkshire RG20 7NN, England, and [c]Sir William Dunn School of Pathology, University of Oxford, South Parks Road, Oxford OX1 3RE, England

Correspondence e-mail: susan.lea@biop.ox.ac.uk

Received 28 April 2006
Accepted 12 July 2006

A construct consisting of residues 10–310 of BipD, a component of the *Burkholderia pseudomallei* type III secretion system (T3SS), has been overexpressed as a GST fusion, cleaved from the GST tag and purified. Crystals were grown of native and selenomethionine-labelled BipD. The crystals grow in two different polymorphs from the same condition. The first polymorph belongs to space group $C222$, with unit-cell parameters $a$ = 103.98, $b$ = 122.79, $c$ = 49.17 Å, a calculated Matthews coefficient of 2.4 Å$^3$ Da$^{-1}$ (47% solvent content) and one molecule per asymmetric unit. The second polymorph belongs to space group $P2_12_12$, with unit-cell parameters $a$ = 136.47, $b$ = 89.84, $c$ = 50.15 Å, and a calculated Matthews coefficient of 2.3 Å$^3$ Da$^{-1}$ (45% solvent content) for two molecules per asymmetric unit (analysis of the self-rotation function indicates the presence of a weak twofold non-crystallographic symmetry axis in this $P2_12_12$ form). The native crystals of both forms give diffraction data to 2.7 Å resolution, while the SeMet-labelled $P2_12_12$ crystals diffract to 3.3 Å resolution. A $K_2PtCl_4$ derivative of the $P2_12_12$ form was also obtained and data were collected to 2.7 Å with radiation of wavelength $\lambda$ = 0.933 Å. The Pt-derivative anomalous difference Patterson map revealed two self-peaks on the Harker sections.

## 1. Introduction

Type III secretion systems (T3SSs) are essential virulence determinants of many Gram-negative bacterial pathogens. The T3SS is required to translocate virulence effectors into the host cell. The T3SS consists of a 'needle complex' composed of an external hollow needle held within a basal body that traverses both bacterial membranes. Secretion is activated by contact of the tip of the needle with host cells, resulting in the formation of a pore in the host-cell membrane that is contiguous with the needle. Other effector proteins are injected *via* this apparatus directly into the host-cell cytoplasm (for a review, see Johnson *et al.*, 2005).

Among Gram-negative bacteria that possess a T3SS, the *Burkholderia* species are highly pathogenic to humans. They have been listed as biological risk category B agents and as a consequence of their infectivity by the respiratory route are considered potential bioterror agents (Rotz *et al.*, 2002). *B. pseudomallei* causes melioidosis in humans, a disease endemic in Southeast Asia and Northern Australia. This disease presents in a variety of ways from subacute and chronic suppurative infections to a rapidly fatal septicaemia (White, 2003). *B. mallei* causes the zoonotic disease glanders, mainly in horses. *B. mallei* can also infect humans, an infection that is almost invariably fatal if untreated (Wilkinson, 1981).

The *B. pseudomallei* needle is composed of the ∼9 kDa protein BsaL, the structure of which has been determined by NMR (Zhang *et al.*, 2006) and is homologous both in sequence and structure to the *Shigella flexneri* needle component MxiH. We have recently determined the crystal structure of MxiH and assembled a molecular model of the T3SS needle, docking its crystal structure into a 16 Å EM reconstruction of the *S. flexneri* needle (Cordes *et al.*, 2005; Deane, Cordes *et al.*, 2006; Deane, Roversi *et al.*, 2006). As part of our ongoing structural effort to further characterize the T3SS needle

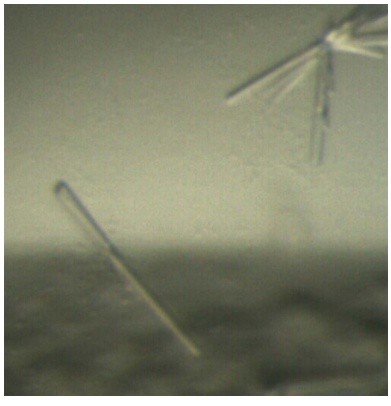

**Table 1**
BipD X-ray diffraction data-collection statistics.

Value in parentheses are for the highest resolution shells.

| | Native 1 | Native 2 | SeMet | $K_2PtCl_4$ soak |
|---|---|---|---|---|
| X-ray source | ESRF ID29 | ESRF ID14-2 | ESRF ID29 | ESRF ID14-2 |
| Detector | ADSC scanner | ADSC scanner | ADSC scanner | ADSC scanner |
| Space group | *C*222 | $P2_12_12$ | $P2_12_12$ | $P2_12_12$ |
| *Z* | 8 | 8 | 8 | 8 |
| Unit-cell parameters | | | | |
| *a* (Å) | 103.98 | 136.47 | 135.90 | 136.52 |
| *b* (Å) | 122.79 | 89.84 | 89.50 | 89.55 |
| *c* (Å) | 49.17 | 50.15 | 49.97 | 49.29 |
| Wavelength (Å) | 0.9778 | 0.9330 | 0.9794 | 0.9330 |
| Resolution limits (Å) | 54–2.6 (2.74–2.6) | 54–2.7 (2.85–2.7) | 43–3.2 (3.37–3.2) | 33–2.7 (2.85–2.7) |
| Completeness (%) | 99.8 (99.8) | 99.8 (99.8) | 100.0 (100.0) | 95.2 (95.2) |
| Anomalous completeness (%) | — | — | 99.9 (99.9) | 95.0 (73.4) |
| Measured reflections | 48047 (6998) | 114952 (8942) | 67849 (10074) | 106839 (9603) |
| Unique reflections | 10006 | 17569 | 10590 | 16408 |
| $I/\sigma(I)$ | 6.1 (1.6) | 7.4 (2.4) | 3.9 (1.8) | 7.7 (2.2) |
| Multiplicity | 4.8 (4.9) | 6.5 (3.6) | 6.4 (6.7) | 6.5 (5.3) |
| $R_{\rm merge}$† | 9.4 (42.7) | 8.7 (31.8) | 16.9 (41.5) | 8.0 (33.1) |
| $R_{\rm anom}$‡ | — | — | 8.3 (3.6) | 4.5 (19.8) |

† $R_{\rm merge} = 100 \times \sum_h [\sum_i |\langle I(h)\rangle - I(h)_i| / \sum_i I(h)_i]$, where $I(h)_i$ is the $i$th observation of reflection $h$ and $\langle I(h)\rangle$ is the mean intensity of all observations of $h$. ‡ $R_{\rm anom} = 100 \times \sum_h |\langle I^+\rangle - \langle I^-\rangle| / \sum_h (\langle I^+\rangle + \langle I^-\rangle)$, where $\langle I^+\rangle$ and $\langle I^-\rangle$ are the mean intensities of the Bijvoet pairs for observation $h$.

machinery, we have now endeavoured to express, purify and crystallize the *B. pseudomallei* BipD protein, a key component of the translocation apparatus in this bacterium. BipD is required for full virulence in murine models of melioidosis and mutation of the *B. pseudomallei bipD* gene impairs invasion of epithelial cells *in vitro* (Stevens & Galyov, 2004; Stevens *et al.*, 2004).

There are no close BipD sequence homologues of known structure, the closest (13% sequence identity) being LcrV (Derewenda *et al.*, 2004), a T3SS component of *Yersinia pestis*, which has been shown to be located at the tip of the T3SS needle and is similarly needed for cell invasion (Mota, 2006). The closest sequence homologues of BipD are *Shigella* IpaD and *Salmonella* SipD (36% and 33% sequence identity to BipD, respectively); together with some enteropathogenic *Escherichia coli* and *Chromobacterium violaceum* proteins, they form the T3SS protein family called 'invasion plasmid antigen IpaD proteins' (Bateman *et al.*, 2004). A three-dimensional structure of *Burkholderia* BipD, together with the structure of *Yersinia* LcrV (Derewenda *et al.*, 2004), should increase our understanding of their role in T3SS pathogenesis.

## 2. Experimental procedures

### 2.1. Protein expression and purification

The construction of the pGEXBipD plasmid used for expression of the GST-BipD fusion protein has been described previously (Stevens *et al.*, 2002). The plasmid was transformed into *E. coli* BL21 strain.

The bacteria were grown in LB at 310 K overnight. 10 ml of the overnight culture was inoculated into 400 ml fresh LB and grown for 2.5 h at 310 K with shaking, induced with 100 µl 1 *M* IPTG and incubated for a further 2.5 h. The bacteria were pelleted by centrifugation, resuspended in 20 ml TBS (10 m*M* Tris–HCl pH 8, 150 m*M* NaCl) and sonicated using a Heat Systems Inc. sonicator Model XL2020 (5 × 10 s sonication followed by 10 s pause) with a half-inch disruptor horn at output setting 4. The debris was removed by centrifugation. 800 µl of a 50% suspension of glutathione Sepharose 4B beads (Amersham) was added to the supernatant and incubated for 30 min at room temperature. The beads were washed three times with TBS. The pelleted beads were resuspended in 200 µl TBS containing 10 units of thrombin (Sigma) and incubated on a rotating-plate mixer for 14 h at room temperature. The supernatant containing released BipD was collected.

The protein was further purified by gel filtration, injecting about 3 ml at a concentration of 0.5 mg ml$^{-1}$ onto an S75 16/60 FPLC column (Amersham) running at 1 ml min$^{-1}$ in 20 m*M* Tris–HCl pH 6.6 and 20 m*M* NaCl running buffer. Six 2 ml fractions containing the protein were collected and concentrated by centrifugation in 10 kDa molecular-weight cutoff Vivaspin centrifugal concentrators (VivaScience, Sartorius Group) to a concentration of 10 mg ml$^{-1}$ at 277 K.

SeMet-labelled BipD was produced by expression in the *E. coli* methionine-auxotrophic strain B834 (DE3). Cultures were grown in LB media to an $A_{600\,\rm nm}$ of 0.2, pelleted (15 min, 4000*g*, 277 K), washed in PBS three times and resuspended in 10 µl SeMet medium without SeMet before being used to inoculate SelenoMet Medium Base containing SelenoMet Nutrient Mix and SeMet stock solution (4 ml per litre; Molecular Dimensions, UK). Cells were grown and induced as described above. SeMet-labelled protein was purified as described above. Full incorporation of selenomethionine was confirmed by mass spectrometry (data not shown).

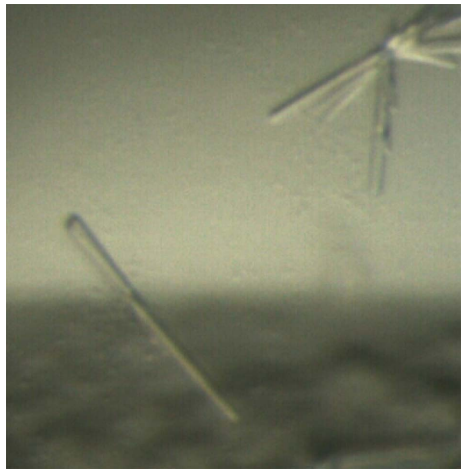

**Figure 1**
Orthorhombic crystals of native BipD. The largest crystal has dimensions of approximately 20 × 20 × 300 µm.

### 2.2. Crystallization

Initial crystallization conditions were obtained by sparse-matrix screening (Jancarik & Kim, 1991) using the sitting-drop vapour-diffusion technique. Drops were prepared by mixing 0.2 µl protein solution (10 mg ml$^{-1}$, 20 m*M* Tris pH 6.6, 20 m*M* NaCl) with 0.2 µl reservoir solution and were equilibrated against 100 µl reservoir solution at 293 K. Initial crystals of BipD grew in two weeks in condition No. 22 of Molecular Dimensions Stura Footprint Screen 1 (1 *M* trisodium citrate, 10 m*M* sodium borate pH 8.5). Subsequent optimization yielded diffraction-quality crystals of BipD (Fig. 1) at citrate concentrations in the range 1.0–1.17 *M* and at pH values between 8.4 and 8.5. Crystals of SeMet-labelled BipD were grown as described above from SeMet-labelled sample. The Pt derivative was obtained by addition of 1 µl reservoir solution saturated with $K_2PtCl_4$ to the 0.4 µl crystallization drop; crystals were soaked for 1 d at 293 K prior to data collection.

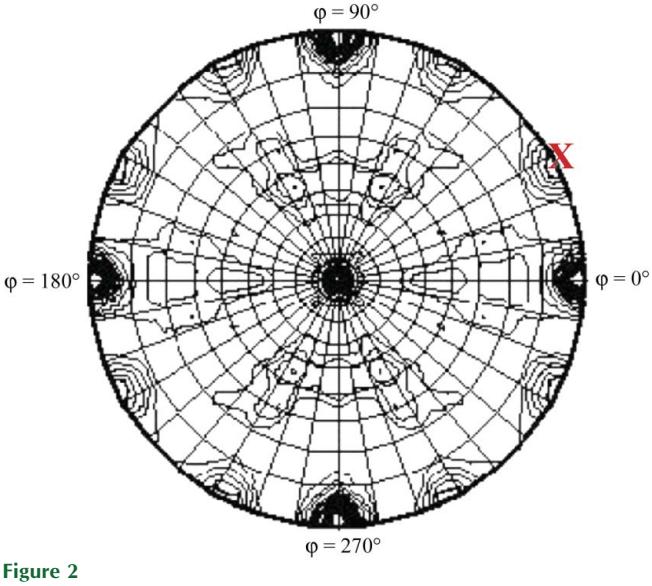


**Figure 2**
The $\kappa = 180°$ section of the self-rotation function calculated for the $P2_12_12$ native data set using *MOLREP* (Collaborative Computational Project, Number 4, 1994) with an integration radius of 27.6 Å and data in the resolution range 37–5 Å. The peak (marked with an X) at $(\omega, \varphi) = (90, 27°)$ represents 46% of the peaks for the crystallographic twofold axes.

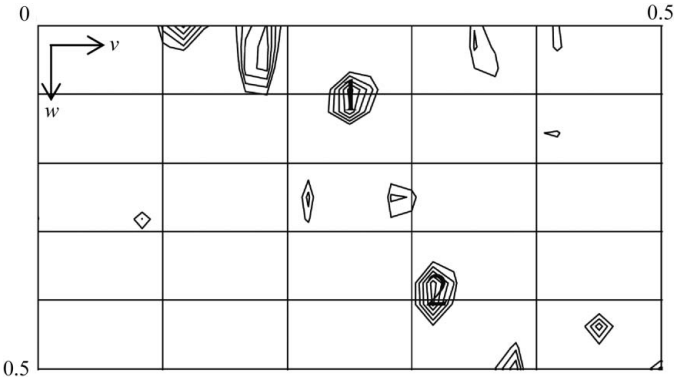


**Figure 3**
Harker section ($u = 0.5$) of the anomalous difference Patterson maps of the $K_2PtCl_4$ soak of BipD (space group $P2_12_12$) calculated at 3.3 Å resolution with data collected at $\lambda = 0.9330$ Å (see Table 1) by *autoSHARP*. Maps are drawn with a minimum contour level of $1.5\sigma$ with $0.3\sigma$ increments. The two main peaks are labelled.

### 2.3. Data collection and processing

Crystals of native and SeMet BipD were cryoprotected in reservoir solution containing 20% glycerol and flash-cryocooled in liquid nitrogen for data collection. The crystal of the Pt derivative of BipD was mounted and flash-cryocooled directly in the cryostream.

Diffraction data were recorded at 100 K (Table 1). Data were indexed and integrated in *MOSFLM* (Leslie, 1992) and scaled with *SCALA* (Evans, 1997) within the *CCP*4 program suite (Collaborative Computational Project, Number 4, 1994). A fluorescence scan measured on the SeMet crystal across the Se edge yielded values of $f' = -8.0$ and $f'' = 6.4$ using the program *CHOOCH* (Evans & Pettifer, 2001).

## 3. Results and discussion

Of all the BipD crystals analysed, all of which were grown under the same conditions and all of which had a similar rod shape, only one belonged to space group *C*222 (labelled Native 1), while all other crystals examined belonged to space group $P2_12_12$.

The *C*222 crystal contains one molecule per asymmetric unit, with a Matthews coefficient of 2.4 Å$^3$ Da$^{-1}$, corresponding to a solvent content of 47% (Matthews, 1968). The $P2_12_12$ crystals are likely to contain two molecules per asymmetric unit, based on the frequency distribution of Matthews coefficients among the PDB entries at comparable resolution (Kantardjieff & Rupp, 2003); this is confirmed by the $P2_12_12$ self-rotation function peak at $\omega = 90$, $\varphi = 27$, $\kappa = 180°$, which has an intensity equal to 46% of the crystallographic peaks (Fig. 2).

The *c* unit-cell parameter is equal to about 49 Å in both BipD crystal forms; the estimated solvent content and unit-cell volumes are very similar ($V$ = 627 744 and 613 596 Å$^3$ for *C*222 and $P2_12_12$, respectively), making it possible that the two lattices are equivalent. Indeed, the cross-crystal rotation function [computed between the *C*222 and $P2_12_12$ forms with the program *ALMN* (Collaborative Computational Project, Number 4, 1994) using data in the resolution range 15–5 Å] has a $5\sigma$ peak at $\omega = 0$, $\varphi = 0$, $\kappa = 26.7°$ (data not shown), suggesting that the two lattices are related by a simple rotation around the direction of the *c* axis. Moreover, this cross-crystal rotation approximately aligns the direction of the *a* axis of *C*222 with the NCS twofold in $P2_12_12$. Thus, the $P2_12_12$ form is likely to be the result of a change in symmetry that causes one of the twofold axes in *C*222 to become an NCS twofold in $P2_12_12$.

Anomalous difference Patterson maps for the Pt and SeMet derivatives were calculated within *autoSHARP* (Vonrhein *et al.*, 2005) using $(E^2 - 1)$ coefficients and strict outlier rejection. The Pt anomalous difference Patterson Harker sections suggest the presence of two sites (Fig. 3), while the SeMet anomalous difference Pattersons for the expected $2 \times 6 = 12$ Se sites are not easily interpretable (data not shown), nor have they yielded a reliable set of Se sites, despite attempts using the available Patterson-solving computer programs. The current phasing strategy is therefore based on initial SIRAS phasing with the Pt sites only, which should enable the location of the subset of ordered Se sites in the SeMet derivative and allow MIRAS phasing with the full BipD native data set and Pt- and SeMet-derivative data sets.

PR is funded by a Wellcome Trust Grant (No. 077082) to SML and PR. SJ is funded by a grant from the Medical Research Council of the UK (G0400389) to SML. JED is funded by an Australian National Health and Medical Research Council CJ Martin Postdoctoral

Fellowship (ID-358785). Work at the IAH is supported by the BBSRC (UK). We are grateful to Ed Lowe and Martin Noble for collecting the diffraction data from the SeMet and $K_2PtCl_4$ derivatives. Marc Morgan and Jenny Gibson assisted us with the use of the crystallization robot. Michael Wood was involved in the cloning of BipD.

## References

Bateman, A., Coin, L., Durbin, R., Finn, R. D., Hollich, V., Griffiths-Jones, S., Khanna, A., Marshall, M., Moxon, S., Sonnhammer, E. L., Studholme, D. J., Yeats, C. & Eddy, S. R. (2004). *Nucleic Acids Res.* **32**, D138–D141.

Collaborative Computational Project, Number 4 (1994). *Acta Cryst.* D**50**, 760–763.

Cordes, F. S., Daniell, S., Kenjale, R., Saurya, S., Picking, W. L., Picking, W. D., Booy, F., Lea, S. M. & Blocker, A. (2005). *J. Mol. Biol.* **354**, 206–211.

Deane, J. E., Cordes, F. S., Roversi, P., Johnson, S., Kenjale, R., Picking, W. D., Picking, W. L., Lea, S. M. & Blocker, A. (2006). *Acta Cryst.* F**62**, 302–305.

Deane, J. E., Roversi, P., Cordes, F. S., Johnson, S., Kenjale, R., Daniell, S., Booy, F., Picking, W. D., Picking, W. L., Blocker, A. J. & Lea, S. M. (2006). *Proc. Natl Acad. Sci. USA*, doi:10.1073/pnas.0602689103.

Derewenda, U., Mateja, A., Devedjiev, Y., Routzahn, K. M., Evdokimov, A. G., Derewenda, Z. S. & Waugh, D. S. (2004). *Structure*, **12**, 301–306.

Evans, G. & Pettifer, R. (2001). *J. Appl. Cryst.* **34**, 82–86.

Evans, P. R. (1997). *Jnt CCP4/ESF–EACBM Newsl. Protein Crystallogr.* **33**, 22–24.

Jancarik, J. & Kim, S.-H. (1991). *J. Appl. Cryst.* **24**, 409–411.

Johnson, S., Deane, J. E. & Lea, S. M. (2005). *Curr. Opin. Struct. Biol.* **15**, 700–707.

Kantardjieff, K. A. & Rupp, B. (2003). *Protein Sci.* **12**, 1865–1871.

Leslie, A. G. W. (1992). *Jnt CCP4/ESF–EACBM Newsl. Protein Crystallogr.* **26**.

Matthews, B. W. (1968). *J. Mol. Biol.* **33**, 491–497.

Mota, L. J. (2006). *Trends Microbiol.* **14**, 197–200.

Rotz, L. D., Khan, A. S., Lillibridge, S. R., Ostroff, S. M. & Hughes, J. M. (2002). *Emerg. Infect. Dis.* **8**, 225–230.

Stevens, M. P. & Galyov, E. E. (2004). *Int. J. Med. Microbiol.* **293**, 549–555.

Stevens, M. P., Haque, A., Atkins, T., Hill, J., Wood, M. W., Easton, A., Nelson, M., Underwood-Fowler, C., Titball, R. W., Bancroft, G. J. & Galyov, E. E. (2004). *Microbiology*, **150**, 2669–2676.

Stevens, M. P., Wood, M. W., Taylor, L. A., Monaghan, P., Hawes, P., Jones, P. W., Wallis, T. S. & Galyov, E. E. (2002). *Mol. Microbiol.* **46**, 649–659.

Vonrhein, C., Blanc, E., Roversi, P. & Bricogne, G. (2005). In *Crystallographic Methods*, edited by S. Doublié. Totowa, NJ, USA: Humana Press.

White, N. J. (2003). *Lancet*, **361**, 1715–1722.

Wilkinson, L. (1981). *Med. Hist.* **25**, 363–384.

Zhang, L., Wang, Y., Picking, W. L., Picking, W. D. & De Guzman, R. N. (2006). *J. Mol. Biol.* **359**, 322–330.